Numerical investigation of pressure pulse predictions for propellers mounted on an inclined shaft

Sixth International Symposium on Marine Propulsors
smp'19, Rome, Italy, May 2019

Numerical Investigation of Pressure Pulse Predictions for Propellers Mounted on an Inclined Shaft

Muye Ge[1], Urban Svennberg[2], Rickard E. Bensow[1]

[1]Division of Marine Technology, Department of Mechanics and Maritime Sciences
[1]Chalmers University of Technology, Gothenburg, Sweden
[2]Kongsberg Hydrodynamic Research Centre, Kongsberg Maritime Sweden AB, Kristinehamn, Sweden

ABSTRACT

In the presented study, two high-skew model scale marine propellers were tested in the cavitation tunnel and the induced pressure pulses were measured during the test. Propeller shaft was inclined about 10 degrees to create blade load variations. The cavitation pattern were recorded using high speed videos. The open-source package OpenFOAM and commercial package Star-ccm+ are used as simulation tools to predict pressure pulses numerically. By using the fully turbulent $SST\ k-\omega$ model, the predicted wetted flow pressure pulse levels agreed well compared to experimental measurements, but together with Schnerr-Sauer cavitation mass transfer model, massive cavitation was predicted which lead to inaccurate pressure pulse predictions. The transition sensitive turbulence model $\gamma - Re_\theta$ model is used to study the cases, and simulation results reveal the existence of laminar-transition zone and vortex structures on the propeller blades. Attempts are made to linking correlation-based separation region from the transition model and the cavitation model, and good predictions of cavitation pattern are achieved but the predicted pressure pulses levels are merely improved.

Keywords

Pressure pulse; URANS; Transition; Cavitation; Marine propeller

1 INTRODUCTION

Pressure pulses induced by an operating marine propeller is one of the major sources of both on board noise and vibrations as well as underwater radiated noise. The rising concern to the comfort of on board crews and passengers and environmental impact to sea creatures thus directs more attention to the accurate prediction of propeller induced pressure pulses. Besides, there is usually a trade off between lower levels of pressure pulse levels and higher propeller efficiency, and a more accurate prediction of pressure pulses could result in more optimal propeller designs.

There are several successful predictions of propeller induced pressure pulses in behind conditions (Paik et al 2013, Fujiyama 2015, Berger et al 2010 and Taskar et al 2017) and many successful predictions of cavitation patterns on propeller blades (Vaz et al 2015, Bensow & Bark 2010 and Gaggero et al 2014) using URANS, LES and(or) BEM. However, with nearly uniform inflow conditions, un-satisfying predictions of cavitation pattern and pressure pulse levels are not rare (Vaz et al 2015, Asnaghi et al 2015).

In the present study, two high-skew model scale marine propellers are considered, here denoted propeller A and propeller B. The two propellers have similar design and propulsion characteristics, while propeller B is slightly tip unloaded. In order to study the influence of different designs on induced pressure pulse levels, experimental measurements were performed and numerical simulations were conducted to analyse the prediction capacities of current numerical methods. The RANS approach with widely used Schnerr-Sauer cavitation model was used in the numerical simulations, and the pressure fluctuations were directly taken from the simulations to analysis the induced pressure pulses.

It is generally believed that with Reynolds number higher than 1,000,000, the influence of laminar-transition effect of the forces on the propeller is small, but the removal of laminar-transition surface flow requires much higher Reynolds number (Gerrit 1981). LES is believed to be one of the promising choice to predict the transition effect but the approach is still under development for this kind of prediction. Apart from other possible approaches, the LCTM (Local Correlation based Transition Modelling) based models which link empirical transition correlations and local determined quantities are suitable choices for the present study, which provide reasonable accuracy for predicting natural transition, bypass transition, separation induced transition and cross flow and surface roughness corrections, like the $\gamma - Re_\theta$ transition model (Langtry & Menter 2009).

Many studies have been conducted regarding propeller open water simulations, and improved predictions of propulsion characteristics were widely reported for non-cavitating conditions using LCTM. The surface flow features are better predicted on the propeller blades with the capture of laminar-transition flow. However, the $\gamma - Re_\theta$ transition model is not linked to the widely used cavitation models which usually assume uniformly distributed nuclei in the water medium and the nuclei would grow once the local pressure is below saturation pressure. The use of transition model usually have a limited influence to the pressure distribution while the pressure distribution is almost the only factor influencing the cavitation prediction. One of the

example is the work conducted by Reverberi et al (2016). Separation induced transition is one of the major mechanisms on the model scale marine propellers triggering turbulent flow. Though the behind mechanisms of sheet cavity inception is still not fully understood, many researchers revealed that the detachment of the sheet cavity usually occurs slightly downstream of the laminar separation point, with some exceptions with detachment inside the transition zone, instead of from the minimum pressure point (Franc & Michel 1985, Franc & Michel 1988, Wang et al 2001, Casey 1974, Arakeri 1975 and Rijsbergen 2017).

The layout of the present paper is as follows. The experimental measurements will be described first together with used numerical methods. The results for non-cavitating conditions will be presented and discussed first. Then the pressure pulses from numerical simulations will be compared to the experimental data as well as cavitation pattern predictions. Lastly an attempt to linking the transition model with cavitation model will be presented.

2 METHODS

In the present study, two high-skew model scale marine propellers were tested in the cavitation tunnel at Kongsberg Hydrodynamic Research Centre. In the experiments, each propeller was mounted on the upstream end of an inclined shaft with 9.8 degrees inclination to create blade load and cavitation pattern variation and also give a simple inflow for the CFD analyses. This set up is different from normal operation for the propeller where the cavitation is triggered by the interaction between the blade and the wake behind the ship. Eight pressure transducers were placed on the wall above the propeller to measure induced pressure fluctuations, with different advance ratios J and cavitation numbers σ, which were chosen to give conditions with and without cavitation. The distance between propeller tip and pressure transducers are ranging from 83mm(No. 3) to 106mm(No. 8). The configurations and pressure transducer arrangements are shown in Figure 1. The transducers No. 1, 3, 6, 8 are located alongside the shaft center line and transducers No. 5, 6, 7 are located on the propeller center line. The Reynolds numbers for the tests were between about 1,000,000 to 1,200,000 based on 0.75 blade chord length. The experimental results show that both in non-cavitating and cavitating conditions, the pressure pulses are rich in 1st and 2nd order BPF (Blade Passing Frequencies). High speed videos show that for the cavitating conditions, the tip vortex cavitation and sheet cavitation could develop through the propeller revolutions. However, it could also be noticed that intermittent sheet cavitation, bubble cavitation and blade root cavitation may develop on the propeller blade suction side, which indicate the pressure is below saturation pressure at these locations. The typical cavitation pattern with $J = 0.85$ and $\sigma = 2.0$ for propeller A and B are shown in Figure. 2.

The open-source package OpenFOAM (v1806+) and commercial code Star-ccm+ (v12.06.010) are used to perform numerical simulations. Flow is assumed to be incompressible in both packages, and second order euler upwind time scheme is used to treat time advancing with fixed time step of 1024 steps per revolution for non-cavitating conditions and 2048 steps per revolution for cavitating conditions. The $SST\ k-\omega$ turbulence model and Schnerr-Sauer cavitation mass transfer model are used in both packages. In OpenFOAM, the PIMPLE algorithm is used for pressure-velocity coupling and in Star-ccm+ the SIMPLE algorithm is used. The convection of turbulence terms are treated using upwind scheme in OpenFOAM and 2nd order upwind scheme in Star-ccm+. The convection of velocity is treated using linearUpwind based on velocity gradient in OpenFOAM and 2nd order upwind scheme in Star-ccm+. The transportation of vapor fraction is treated using upwind scheme without any compression terms in both packages. For the gradient calculation, linear interpolation with Gauss theorem is used without any limiters in OpenFOAM.

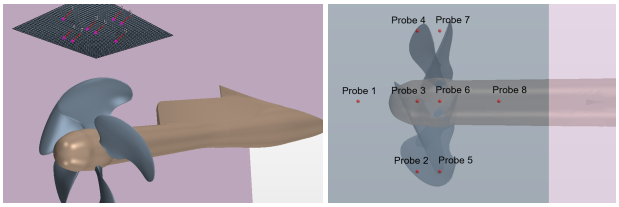

Figure 1: Test configurations and pressure transducer arrangements

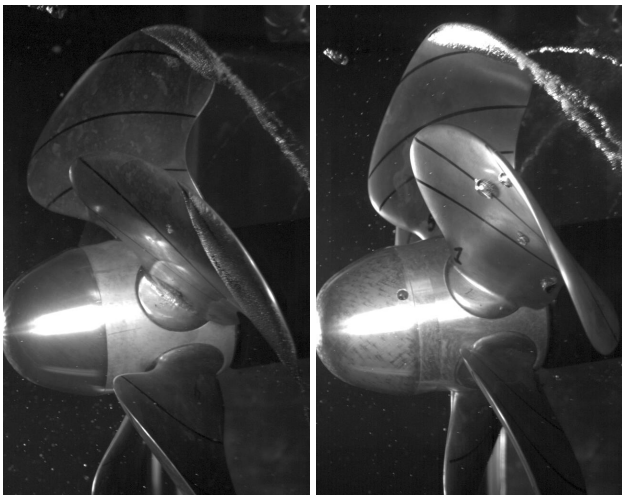

Figure 2: Typical cavitation visualizations of propeller A (left) and B (right) with $J = 0.85$ and $\sigma = 2.0$

The $\gamma - Re_\theta$ transition model is also used in OpenFOAM for certain conditions. The fundamental correlation of the transition model is the linking of scaled ratio of vorticity Reynolds number $Re_v = \frac{\rho y^2}{\mu} S$ and momentum thickness Reynolds number Re_θ with the boundary layer shape factor H as $\frac{max(Re_y)}{2.193 Re_\theta} \sim H$. Similarly $\frac{Re_v}{3.235 Re_{\theta c}} > 1$ is used to account for shape factor H higher than 3.5, which is the correlated laminar separation criteria. For the full details of the model we refer to (Langtry & Menter 2009).

Several meshes have been generated to study the present cases. The major meshes for the two propellers are gener-

ated using Pointwise which is referred to OFF mesh in the present study. The meshes consist of two regions, one is the inner propeller rotation region and one is the outer tunnel region. Mesh refinements were applied at each blade tip vortex region. The target y+ is 1, and 36 layers are extruded from the structure-meshed blade surface using the hyperbolic extrusion option. For the first 15 layers the growth ratio is set to 1.1 to make sure a suitable boundary layer mesh for the use of transition models. Tetrahedral cells are used to fill out the other space. The summary of the two OFF grids for propeller A and propeller B are shown in Table 1 and 2.

Table 1: Grid summary of OFF mesh, propeller A

Region	Tets	Pyramids	Prisms	Hexes	Total
Inner	11.7m	0.4m	0.2m	10.1m	22.4m
Outer	2.1m	0.1m	0.1m	1.6m	3.9m
Total	13.8m	0.5m	0.3m	11.7m	26.3m

Table 2: Grid summary of OFF mesh, propeller B

Region	Tets	Pyramids	Prisms	Hexes	Total
Inner	15.5m	0.4m	0	10.2m	26.1m
Outer	2.1m	0.1m	0.1m	1.6m	3.9m
Total	17.6m	0.5m	0.1m	11.8m	30.0m

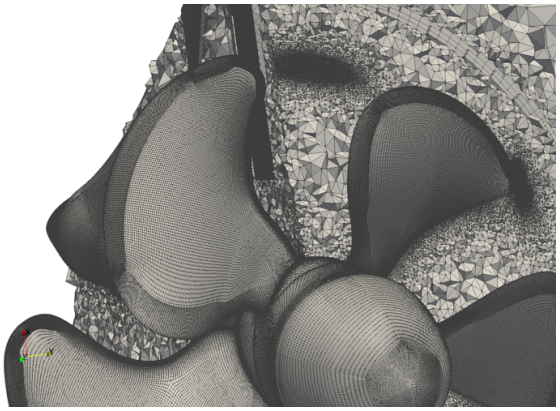

Figure 3: View of near-blade OFF mesh, propeller A

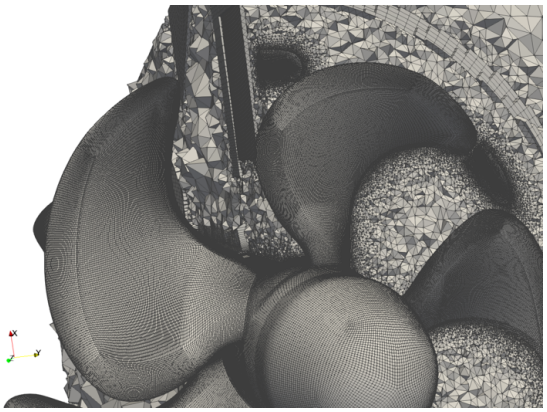

Figure 4: View of near-blade OFF mesh, propeller B

Mesh study is performed for non-cavitating conditions of propeller A. Another four meshes of inner propeller region are generated systematically using Star-ccm+ build-in polyhedral mesher. Target y+ is one for all the meshes with same number of prism layers and growth ratio while the surface mesh and volume mesh are refined accordingly. The brief summary of the four Star-ccm+ meshes are shown in Table 3. The Star-ccm+ fine mesh is shown in Figure 5.

Table 3: Grid summary of Star-ccm+ meshes

Star-ccm+ meshes	Inner	Outer	Total
C (coarse)	3.6m	3.6m	7.2m
Mo (moderate)	7.2m	3.6m	10.8m
M (medium)	12.0m	3.6m	15.6m
F (fine)	18.0	3.6m	21.6m

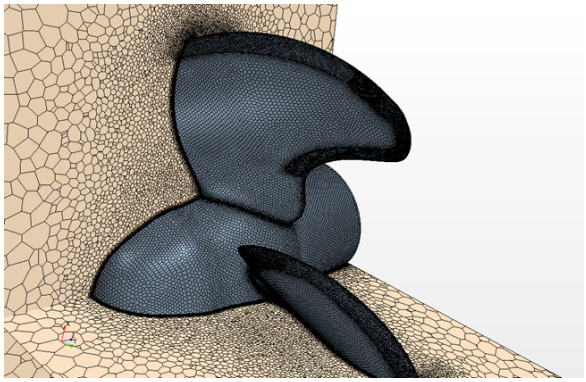

Figure 5: Star-ccm+ F mesh, propeller A

3 SIMULATION RESULTS

3.1 Non-cavitating conditions

For the non-cavitating conditions, the predicted 1st order BPF pressure pulse levels at different pressure transducers are shown in Figure 6 and Figure 7 for propeller A and propeller B respectively, with three different advance ratio J. The values are shown as model-scale values, i.e. the pressure signals are directly used for FFT without any kind of scaling. Comparing to experimental measurements, the pressure pulse levels predicted by numerical simulations are slightly under-predicted with about 5% to 15% but still rather satisfying. The worst prediction were found on pressure transducer No. 3 and No. 6 which are located on the shaft center line. The propeller load decrease with the increase of J, and the predicted pressure pulse levels are decreasing as well in the same trend with experimental measurements. For the non-cavitating conditions, both the experiments and numerical simulations show lower generated pressure pulses by propeller B than propeller A.

In Figure 8, the predicted 1st order BPF pressure pulse levels with different meshes using Star-ccm+ are summarized. The studied condition is propeller A with advance ratio 0.85 under non-cavitating condition. The predicted pressure pulse levels are highly similar with very small differences between the meshes. For the C (coarse) mesh the propeller rotation region consists of 3.2 million cells but the predicted pressure pulse levels are as good as the finest

OFF mesh with tip refinement which clearly have a much better capture of blade surface features and tip vortex.

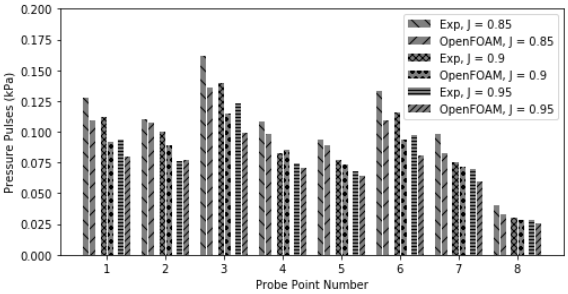

Figure 6: OpenFOAM results, 1st BPF pressure pulses, non-cavitating , propeller A

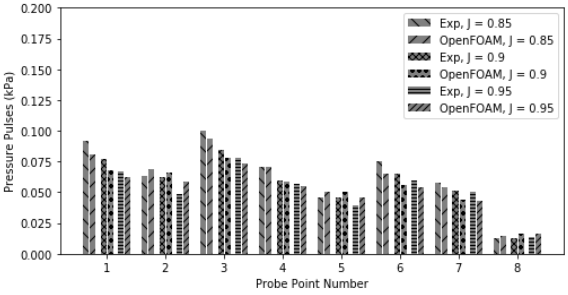

Figure 7: OpenFOAM results, 1st BPF pressure pulses, non-cavitating , propeller B

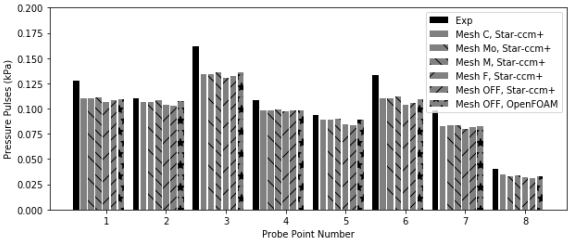

Figure 8: Predicted pressure pulse levels by different meshes, J=0.85, non-cavitating

The propulsion performance of a propeller could be evaluated using non-dimensional thrust and torque coefficients K_T and K_Q under different advance ratio J which are defined as

$$K_T = \frac{T}{\rho n^2 D^4}, \quad K_Q = \frac{Q}{\rho n^2 D^5}, \quad J = \frac{V}{nD},$$

where T and Q represent propeller thrust and torque, ρ represent fluid density, n represent rotation speed in rps and D represent propeller diameter. The relative differences of numerical predicted K_T and K_Q to experimental measurements are shown in Table 4. There are some differences between the two packages OpenFOAM and Star-ccm+ but the difference is rather small. The prediction of propulsion characteristics are acceptable with about $2\% \sim 3\%$ underprediction of the thrust coefficient by using the $SST\ k-\omega$ turbulence model. The results by using $\gamma - Re_\theta$ transition model are also shown here. There is a well-known requirement of using the transition model which is the free-stream turbulent intensity level Tu, but the Tu level is not really known in the experiments. Thus three different free-stream Tu are assumed in the present study, which are 5%, 0.5% and 0.1%. When the transition model is coupled with the SST model, the decay of free-stream Tu is quite significant thus the decay control is applied to maintain the target Tu values around the propeller leading edge. The use of transition model predicts higher values of thrust and the predicted values are highly influenced by the free-stream Tu. For the condition with $Tu = 0.1\%$, the predicted thrust is almost 4% higher than the value predicted by the $k-\omega SST$ model which is significant. However, there is almost no influence to the predicted pressure pulse levels, as shown in Figure 9.

Table 4: Predicted relative differences of force coefficients for propeller A, J=0.85, non-cavitating

J=0.85	Mesh	rdKT	rdKQ	Turbulence model
OpenFoam	OFF	-1.9	-0.1	$SST\ k-\omega$
Star-ccm+	OFF	-2.7	-0.5	$SST\ k-\omega$
Star-ccm+	C	-3.0	-0.7	$SST\ k-\omega$
Star-ccm+	Mo	-3.1	-1.1	$SST\ k-\omega$
Star-ccm+	M	-3.2	-1.2	$SST\ k-\omega$
Star-ccm+	F	-2.6	-0.7	$SST\ k-\omega$
OpenFOAM	OFF	2.8	0.4	$\gamma - Re_\theta$ (Tu=0.1%)
OpenFOAM	OFF	2.5	0.5	$\gamma - Re_\theta$ (Tu=0.5%)
OpenFOAM	OFF	-1.6	0.03	$\gamma - Re_\theta$ (Tu=5%)

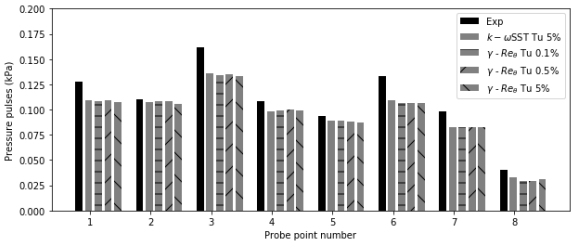

Figure 9: Predicted 1st BPF pressure pulse levels by $SST\ k-\omega$ turbulence model and $\gamma - Re_\theta$ transition model with different free-stream Tu

For non-cavitating condition, the major source of 1st BPF pressure pulses is the pressure distribution close to the blade tip and its spacial location while rotating, which induce pressure fluctuations on the pressure transducers mounting on the top plate. The pressure distribution on the propeller blades predicted by different simulations are shown in Figure 10 with advance ratio $J = 0.85$. Three lines at 0.5R, 0.7R and 0.9R are marked on the propeller blades. The four sub-figures are predicted by $SST\ k-\omega$ model with $Tu = 5\%$, $\gamma - Re_\theta$ transition model with $Tu = 5\%, 0.5\%$ and 0.1%. The lower limit of the color legend is set to saturation pressure. The predicted pressure distributions show no fundamental difference thus little influence could be found regarding pressure pulse predictions. In the same order, the predicted wall shear stress, iso-

surface of Q criterion equals 4×10^6 are shown in Figure 11 and Figure 12. By looking at the wall shear stress contours, it could be found there are limited laminar-transition zone with free-stream $Tu = 5\%$ and for the other two lower free-stream Tu cases the laminar-transition effect almost covers the whole blade suction side. Another noticeable difference is the vortex structures on the blade surface, especially around 0.8R, a series of strong vortices are predicted by the transition model. It's worth to mention that there is not much difference for the tip vortex predictions.

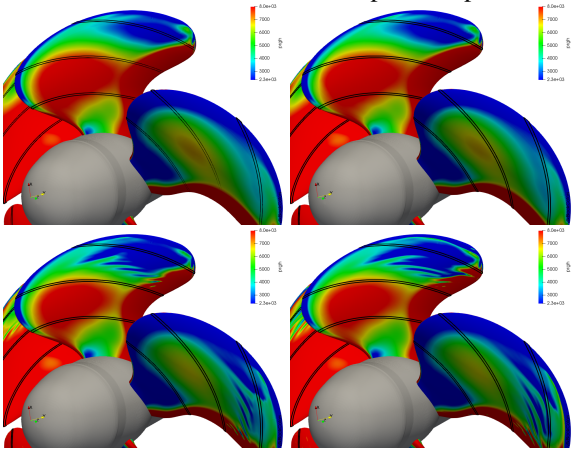

Figure 10: Predicted pressure distribution, propeller A

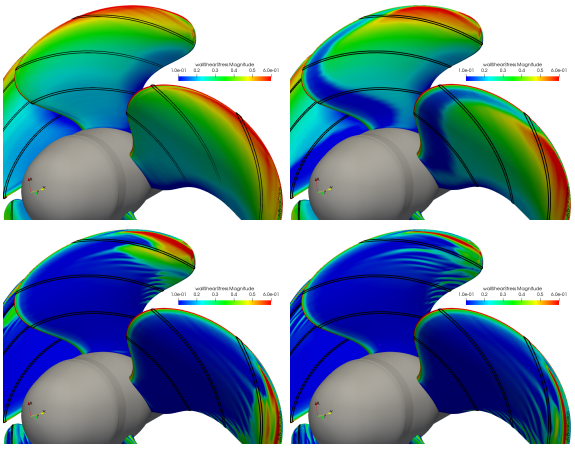

Figure 11: Wall shear stress on propeller blade, propeller A

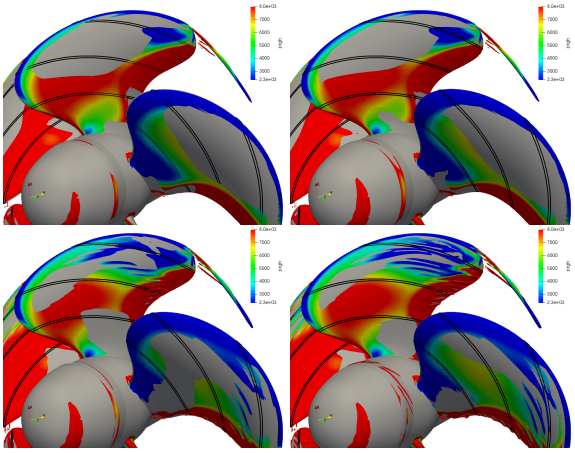

Figure 12: Iso-surface of Q = 4e6, propeller A

3.2 Cavitating conditons

For the cavitating condition, the predicted 1st order BPF pressure pulse levels using $SST\ k-\omega$ turbulence model and Schnerr-Sauer cavitation model for the two propellers with $J = 0.85$ and $\sigma = 2$ are summarized in Figure 13 and Figure 14, where the cavitation number is defined as $\sigma = \frac{P-P_V}{0.5\rho V^2}$. The simulation predicted values are rather off from experimental measurements for propeller A but generally better for propeller B. OpenFOAM and Star-ccm+ predicted similar results. If comparing the two propellers, experimental measurement show propeller B has lower value of pressure pulse levels. But in the numerical simulations propeller A has lower values of pressure pulses which contradict with experimental results.

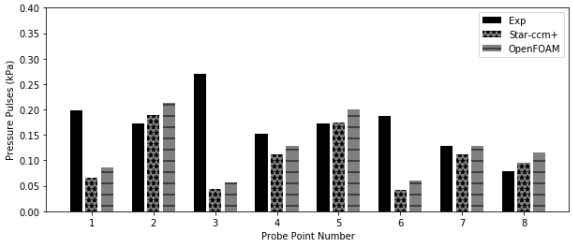

Figure 13: Predicted pressure pulse levels, J=0.85, $\sigma = 2$, propeller A

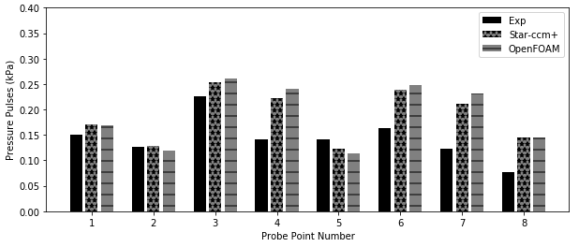

Figure 14: Predicted pressure pulse levels, J=0.85, $\sigma = 2$, propeller B

If looking at the predicted cavitation pattern as shown in Figure 15 and Figure 16, actually for both propellers the numerical simulations predicted massive cavitation which covers almost the whole blades. Even though the predicted pressure pulse levels seems to be good for propeller B, actually the predicted cavitation pattern is even worse compared to high speed video recordings as shown in Figure 17 and Figure 18.

Combining with the predicted pressure distribution under non-cavitating condition as shown in Figure 10, it could be seen that the pressure at leading edge of the displayed propeller blades is below saturation pressure. When using the Schnerr-Sauer cavitation model, all the regions with predicted pressure below saturation pressure will become cavitating, and the cavity will start to develop from the leading edge and finally covers the whole blades. The developing bubbles in the 3rd frame in Figure 17 and the 2nd frame in Figure 18 indicate that a large area of pressure below saturation pressure do exist in the experiments, but sheet cavity didn't develop, while sheet cavity are predicted at these lo-

cations by the numerical codes.

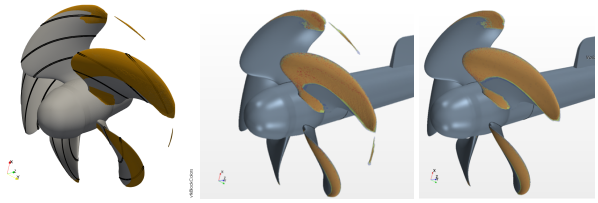

Figure 15: Predicted cavitation pattern, propeller A; from left to right: OpenFOAM OFF mesh, Star-ccm+ OFF mesh, Star-ccm+ F mesh. $J = 0.85$, $\sigma = 2$

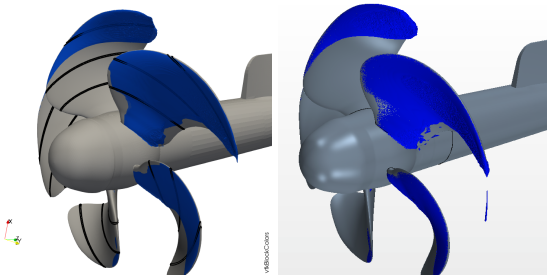

Figure 16: Predicted cavitation pattern, propeller B. left: OpenFOAM OFF mesh; right: Star-ccm+ OFF mesh. $J = 0.85$, $\sigma = 2$

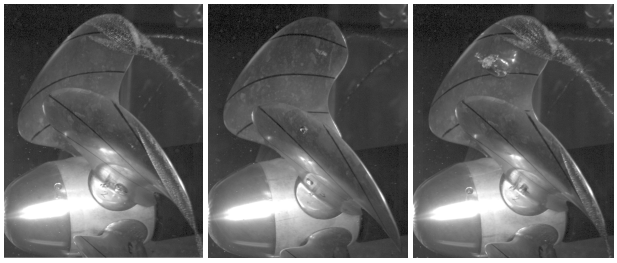

Figure 17: Recorded cavitation pattern from high speed videos, propeller A, $J = 0.85$ and $\sigma = 2$

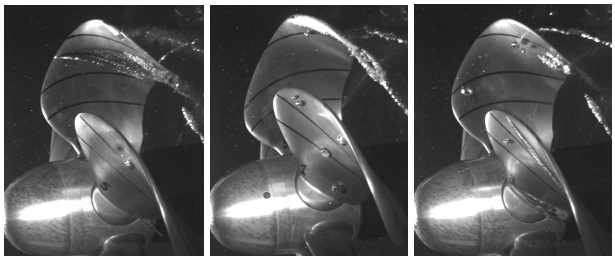

Figure 18: Recorded cavitation pattern from high speed videos, propeller B, $J = 0.85$ and $\sigma = 2$

Apparently the forming up of blade surface vortex structures could influence the boundary layer development and its shape factor, as predicted by using the transition model shown for non-cavitating conditions in Figure 12. Based on the correlation of vorticity Reynolds number and boundary layer shape factor, an indication of laminar separation could be calculated, which is called laminar separation indicator (SepInd) in the present study. The blade surface contours of SepInd are shown in Figure 19. The figures indicate two types of strong laminar separation exist on the propeller suction side: one is located close to the blade tip starting at about $\sim 0.93R$ which is the leading edge main vortex; the other type is a series of blade surface rolling-ups located at around $\sim 0.8R$ starting around $0.2 \sim 0.5$ chord length according to different free-stream Tu. Besides, close to the trailing edge due to the blade curvature some signs of laminar separation could also be found, as well as indications showing up at the blade root. There is no painting test performed for the studied two propellers for validation, but this kind of blade surface vortex structures could be found in many painting tests especially for high-skew propellers.

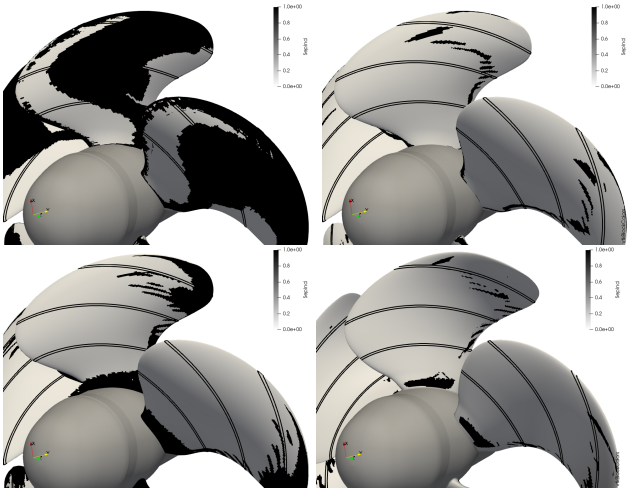

Figure 19: Laminar separation indicator with wetted flow and $J = 0.85$, propeller A with $Tu = 5\%$, $Tu = 0.5\%$, $Tu = 0.1\%$ and propeller B with $Tu = 0.1\%$

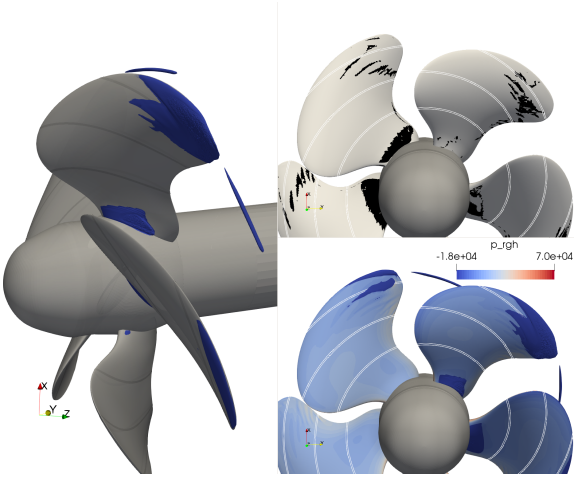

Figure 20: Predicted vapor structures, separation indicator and pressure distribution, propeller A, position 1; $\sigma = 2$

By introducing the laminar separation indicator as another vaporization criterion, the predicted cavitation pattern (iso-surface of $\alpha = 0.5$), laminar separation indicator and pressure distribution on the blade surface are shown in Figure 20 to Figure 23. Two blade positions are shown here where position 2 is the one to match with experimental figures. Tu is set to 0.1%. The prediction of vapor structure is much improved compared with using the original $SST\ k-\omega$ turbulence model and Schnerr-Sauer model. The leading edge vortex located around $\sim 0.93R$ cause the typical sheet

cavity structure for propeller A and the possibly developed strip of cavity created by blade surface vortex structures located around $0.8R$. On the other parts of blade surface no sheet cavitation developed and the pressure remains below saturation pressure.

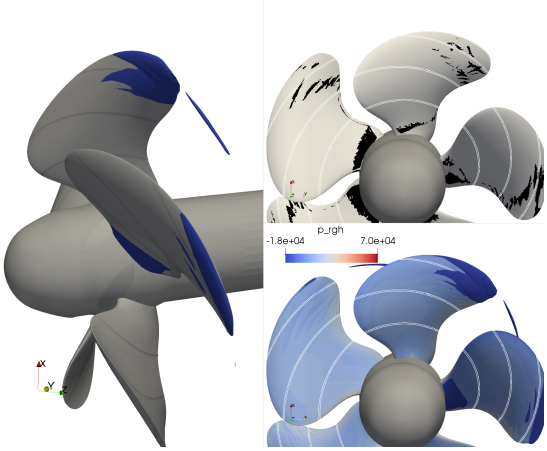

Figure 21: Predicted vapor structures, separation indicator and pressure distribution, propeller A, position 2; $\sigma = 2$

For propeller B, similar improved cavitation predictions could be found. In the experiments, three major types of cavitation pattern could be found, as the three sub-figures shown in Figure 18. The first type is as shown in the first figure, sheet cavity starts forming up at around 0.8R and rarely combined with the second type tip sheet cavity which is shown in the second figure. The third figure shows almost no sheet cavitation on the blade which happens irregularly. In the numerical simulations, the predicted cavitation pattern seems to be the combination of partly cavitation type 1 and type 2. Even though visually a single vapor structure is predicted on each blade, the separation indicator on the propeller blade demonstrate there are two regions of vaporization, one is located around 0.93R and one is from mid-chord 0.8R.

However, with the improved vapor structure predictions by introducing the laminar separation indicator for the cavitation model, the prediction of pressure pulse levels are merely improved, which are summarized in Figure 24. From the experimental side, the cavitation pattern on each blade at different revolutions are overly irregular. For the numerical simulations, the RANS approach is used and uniformly distributed nuclei in water medium is assumed which is clearly unable to capture the same effect observed in the experiments. Regarding the propeller induced pressure pulses, the blade load variation could be predicted reasonably as shown in the present study. For the cavitation induced pressure pulses, two major factors are dominating: the first one is the variation of cavitation, which could be related as the second order time derivative of vapor volume; the second one is the spatial distribution of the first factor. By using the laminar separation indicator, the prediction of vapor structures are significantly improved for the present cases, but the implementation is coupled with vaporization quantitatively but not qualitatively; and due to the limitation of the high speed video camera's angle it is hard to determine if the starting or collapsing of vapor structure is correctly predicted.

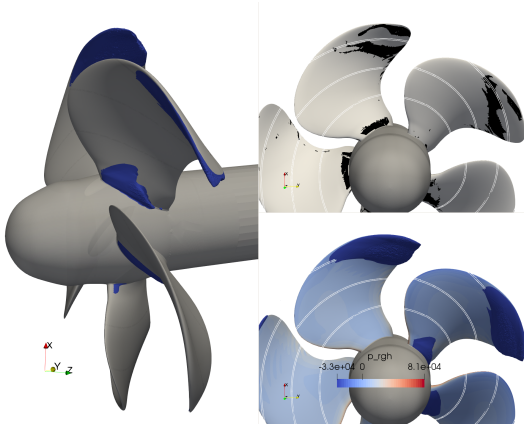

Figure 22: Predicted vapor structures, separation indicator and pressure distribution, propeller B, position 1; $\sigma = 2$

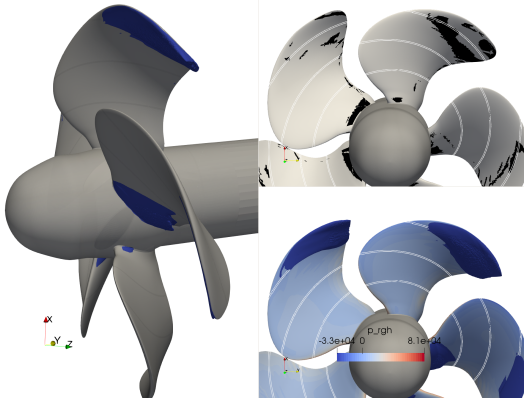

Figure 23: Predicted vapor structures, separation indicator and pressure distribution, propeller B, position 2; $\sigma = 2$

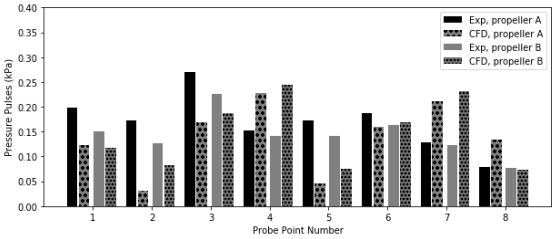

Figure 24: Predicted 1st order BPF pressure pulse levels for propeller A and propeller B by using correlation based laminar separation indicator combined with Schnerr-Sauer cavitation model, $J = 0.85$, $\sigma = 2.0$

SUMMARY AND CONCLUSIONS

In the present study, numerical simulations have been performed for the prediction of model scale marine propeller induced pressure pulses and compared to the experimental measurements. OpenFOAM is used as the major package for simulations and Star-ccm+ is partly used for comparison and mesh study.

The $SST\ k-\omega$ turbulence model and Schnerr-Sauer cavitation model are used for numerical simulations first. The predicted pressure pulse levels for non-cavitating flows agreed well with experimental data, with about $5\% \sim 15\%$ under-prediction. Tip region refinements provide better

captures of tip vortex forming up and tip vortex cavitation, but little impact was found for induced 1st BPF pressure pulses. A very coarse mesh with 3.6 million cells for the propeller rotation region provides the same level of accuracy regarding 1st BPF pressure pulse prediction in non-cavitating condition. For the cavitating flows, the predicted cavitation covers almost all the suction side of the blade which is massively over-prediction compared to high speed videos recorded during the experiments. Large areas of pressure below saturation pressure are predicted in the simulations, while growing bubbles could be found at these areas in the experiments, which indicate pressure is below saturation pressure but sheet cavity didn't develop as predicted by numerical simulations. The difference between OpenFOAM and Star-ccm+ predictions exist but the difference is very small for both non-cavitating and cavitating conditions.

The $\gamma - Re_\theta$ transition model is used for further analysis. Three different free-stream turbulent intensity levels have been studied for the non-cavitating flow. For the wetted flow conditions, compared to the usage of $SST\ k-\omega$ turbulence model, higher thrust coefficients are predicted; predicted pressure distribution on blade surfaces are similar and almost no influence on the predicted 1st BPF pressure pulse levels. Vortex structures are predicted on the blade surface and their locations show strong dependence with free-stream turbulence intensity level. Regions of laminar separation are marked based on empirical correlations and coupled with cavitation mass transfer model, and significantly improved cavitation patterns are predicted. However, the pressure pulse levels are merely improved.

ACKNOWLEDGEMENTS

Financial support for this work has been provided by Kongsberg Maritime Sweden AB through the University Technology Centre in Computational Hydrodynamics hosted at the Department of Mechanics and Maritime Sciences at Chalmers University of Technology. The computations were performed on resources at Chalmers Centre for Computational Science and Engineering (C3SE) provided by the Swedish National Infrastructure for Computing (SNIC).

REFERENCES

Arakeri, V. H. (1975). 'Viscous effects on the position of cavitation separation from smooth bodies'. Journal of Fluid Mechanics **68**(4), pp. 779–799.

Asnaghi, A., Feymark, A. & Bensow, R. E. (2015). 'Computational analysis of cavitating marine propeller performance using OpenFOAM'. Proceedings of the 4th International Symposium on Marine Propulsors, Austin, USA.

Bensow, R. E. & Bark, G. (2010). 'Implicit LES predictions of the cavitating flow on a propeller'. Journal of fluids engineering **132**(4).

Berger, S., Gosda, R., Scharf, M., Klose, R., Greitsch, L. & Abdel-Maksoud, M. (2016). 'Efficient Numerical Investigation of Propeller Cavitation Phenomena causing Higher-Order Hull Pressure Fluctuations'. Proceedings of the 31st Symposium on Naval Hydrodynamics, Monterey, USA.

Casey, M. V. (1974). 'The inception of attached cavitation from laminar separatiohn bubbnles on hydrofoils'. Proceedings of Conference on Cavitation, Edinburgh, England.

Franc, J. P. & Michel, J. M. (1985). 'Attached cavitation and the boundary layer: experimental investigation and numerical treatment'. Journal of Fluid Mechanics **154**, pp. 63–90.

Franc, J. P. & Michel, J. M. (1988). 'Unsteady attached cavitation on an oscillating hydrofoil'. Journal of Fluid Mechanics **193**, pp. 171–189.

Fujiyama, K. (2015). 'Numerical Simulation of Ship Hull Pressure Fluctuation Induced by Cavitation on Propeller with Capturing the Tip Vortex'. Proceedings of the 4th International Symposium on Marine Propulsors, Austin, USA.

Gaggero, S., Tani, G., Viviani, M. & Conti, F. (2014). 'A study on the numerical prediction of propellers cavitating tip vortex'. Ocean Engineering **92**, pp. 137–161.

Kuiper, G. (1981). 'Cavitation inception on ship propeller models'. Thesis, Technical University Delft.

Langtry, R. B. & Menter, F. R. (2009). 'Correlation-based transition modeling for unstructured parallelized computational fluid dynamics codes'. AIAA journal **47**(12), pp. 2894–2906.

Paik, K. W., Park, H. G. & Seo, J. (2013). 'RANS simulation of cavitation and hull pressure fluctuation for marine propeller operating behind-hull condition'. International Journal of Naval Architecture and Ocean Engineering **5**(4), pp. 502–512.

Rijsbergen, M. (2016). 'A review of sheet cavitation inception mechanisms'. Proceedings of the 16th International Symposium on Transport Phenomena and Dynamics of Rotating Machinery, Hawaii, Honolulu.

Reverberi, A., Lloyd, T. & Vaz, G. (2016). 'Towards cavitation modelling accounting for transition effects'. Proceedings of the 19th Numerical Towing Tank Symposium, St. Pierre d'Oleron, France.

Taskar, B., Steen, S. & Eriksson, J. (2017). 'Effect of waves on cavitation and pressure pulses of a tanker with twin podded propulsion'. Applied Ocean Research **65**, pp. 206–218.

Vaz, G., Hally, D., Huuva, T., Bulten, N., Muller, P., Becchi, P., Jose, L. R., Whitworth, S., Macé, R. & Korsström, A. (2015). 'Cavitating flow calculations for the E779A propeller in open water and behind conditions: code comparison and solution validation'. Proceedings of the 4th International Symposium on Marine Propulsors, Austin, USA.

Wang, G.,Senocak, I., Shyy, W. Ikohagi, T. & Cao, S. (2001). 'Dynamics of attached turbulent cavitating flows'. Progress in Aerospace sciences **37**(6), pp. 551-581.